Modeling the Active Sites of Metalloenzymes. 4. Predictions of the Unready States of [NiFe] *Desulfovibrio gigas* Hydrogenase from Density Functional Theory

Shuhua Li and Michael B. Hall*

Department of Chemistry, Texas A&M University, College Station, Texas 77843

Received February 17, 2000

Density functional theory has been used to predict the structures of a variety of active site models for the unready states, **Ni-A** and **Ni-SU**, of the [NiFe] hydrogenase from *Desulfovibrio gigas*. By comparing available experimental results on **Ni-A**, **Ni-SU**, and **Ni-SI** with the computational results on these model complexes, we have been able to identify the most likely formulas and structures for the active sites of **Ni-A** and **Ni-SU**. **Ni-A** is predicted to be a Ni(III)−Fe(II) species with the bridging hydroxo ligand, rather than the expected oxo ligand, while **Ni-SU** is predicted to be a Ni(II)−Fe(II) species with a water molecule coordinated to the Fe center. Both have one of the terminal S atoms (cysteines) protonated.

Introduction

Hydrogenases are enzymes that catalyze the reversible reaction $H_2 \leftrightarrow 2H^+ + 2e^-$. The [NiFe] hydrogenase from *Desulfovibrio (D.) gigas*, as aerobically isolated in the inactive form, has been characterized by X-ray crystallography, at 2.85 Å[1] and 2.54 Å[2] resolution. From these crystallographic analyses and infrared (IR) spectroscopic studies,[3,4] an image of the active site of the oxidized form of [NiFe] *D. gigas* hydrogenase has emerged, as shown in Figure 1. It should be noted that the additional bridging ligand between Fe and Ni (X ligand in Figure 1) is not known for certainty; μ-oxo or hydroxo has been suggested.[1−4]

EPR[5−9] and IR[2,4] experiments showed that the *D. gigas* enzyme can exist in six different redox states, called **Ni-A**, **Ni-B**, **Ni-SU**, **Ni-SI**, **Ni-C**, and **Ni-R**. The crystals used for the X-ray structure determination of the enzyme were grown from a solution that was mainly **Ni-A**. A proposed activation and catalytic cycle[4,10−14] is given in Scheme 1, where each state is tagged with its CO stretching frequency. EPR measurements[5−9] showed that **Ni-A**, **Ni-B**, and **Ni-C** are $S = {}^1/_2$ states, where the simplest interpretation involves one unpaired electron on Ni, while **Ni-SU**, **Ni-SI**, and **Ni-R** are $S = 0$ species. From Scheme

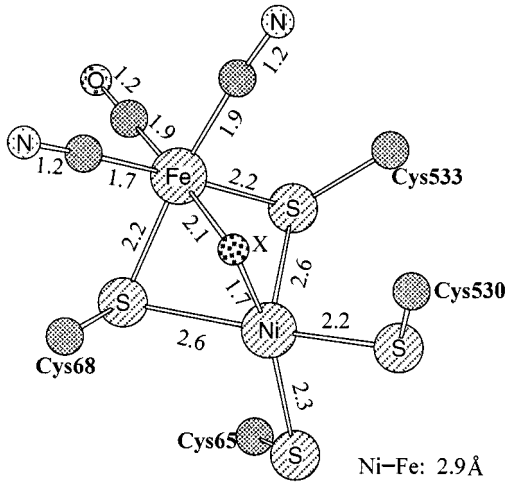

Figure 1. X-ray crystal structure of [NiFe] *D. gigas* hydrogenase.[1,2] The bridging X ligand may be oxo or hydroxo.

Scheme 1

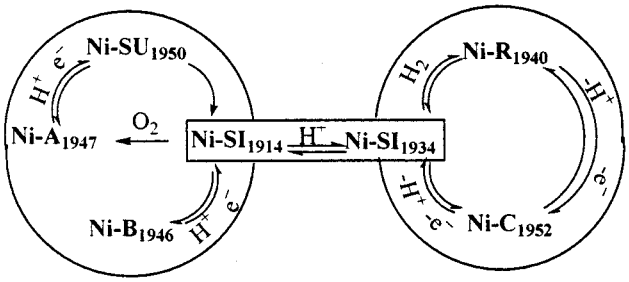

(1) Volbeda, A.; Charon, M. H.; Piras, C.; Hatchikian, E. C.; Frey, M.; Fontecilla-Camps, J. C. *Nature* **1995**, *373*, 580.
(2) Volbeda, A.; Garcin, E.; Piras, C.; de Lacey, A. L.; Fernandez, V. M.; Hatchikian, E. C.; Frey, M.; Fontecilla-Camps, J. C. *J. Am. Chem. Soc.* **1996**, *118*, 12989.
(3) Happe, R. P.; Roseboom, W.; Pierik, A. J.; Albracht, S. P. J.; Bagley, K. A. *Nature* **1997**, *385*, 126.
(4) de Lacey, A. L.; Hatchikian, E. C.; Volbeda, A.; Frey, M.; Fontecilla-Camps, J. C.; Fernandez, V. M. *J. Am. Chem. Soc.* **1997**, *119*, 7181.
(5) Albracht, S. P. J. *Biochim. Biophys. Acta* **1994**, *1188*, 167.
(6) Moura, J. J. G.; Moura, I.; Huynh, B. H.; Krüiger, H. J.; Teixeira, M.; Du Varney, R. G.; Der Vartanian, D. G.; Ljungdahl, P.; Xavier, A. V.; Peck, H. D., Jr.; LeGall, J. *Biochem. Biophys. Res. Commun.* **1982**, *108*, 1388.
(7) Cammack, R.; Patil, O. S.; Hatchikian, E. C.; Fernandez, V. M. *Biochim. Biophys. Acta* **1987**, *912*, 98.
(8) Fernandez, V. M.; Hatchikian, E. C.; Cammack, R. *Biochim. Biophys. Acta* **1985**, *832*, 69.
(9) Fernandez, V. M.; Hatchikian, E. C.; Patil, D. S.; Cammack, R. *Biochim. Biophys. Acta* **1986**, *883*, 145.
(10) Roberts, L. M.; Lindahl, P. A. *Biochemistry* **1994**, *33*, 14339.
(11) Roberts, L. M.; Lindahl, P. A. *J. Am. Chem. Soc.* **1995**, *117*, 2565.
(12) Teixeira, M.; Moura, I.; Xavier, A. V.; Der Vartanian, D. V.; LeGall, J.; Peck, H. D., Jr.; Huyhn, B. H.; Moura, J. J. G. *Eur. J. Biochem.* **1983**, *130*, 481.
(13) Dole, F.; Fournel, A.; Magro, V.; Hatchikian, E. C.; Bertrand, P.; Guigliarelli, B. *Biochemistry* **1997**, *36*, 7847.
(14) Marganian, C. A.; Vazir, H.; Baidya, N.; Olmstead, M. M.; Mascharak, P. K. *J. Am. Chem. Soc.* **1995**, *117*, 1584.

10.1021/ic0001715 CCC: $20.00
Published on Web 12/07/2000

1, one can see that the **Ni-A**, **Ni-SU**, and **Ni-B** are involved in activation/inactivation processes of the enzyme, whereas the **Ni-SI** (**SI_{1914}** and **SI_{1934}**), **Ni-R**, and **Ni-C** participate actively in the catalytic cycle of the *D. gigas* hydrogenase. Furthermore, **Ni-A** and **Ni-SU** are called unready states[4,8] because they need long incubation under H_2 (or a reductant) for activation, while **Ni-B** is called the ready state[4,8] because it is activated rapidly.

Determination of the molecular structures of the six redox states is crucial to understanding the activation and catalytic mechanism of the enzyme. Combinations of experimental methods such as X-ray absorption, ENDOR, EPR, and IR spectroscopies have provided some insight into the nature of these redox states. The IR spectra in the ν(CO) and ν(CN) regions of these species were obtained by reductive activation of the as-purified enzyme with molecular hydrogen and subsequent controlled oxidation.[4] These IR experiments indicated that the transition from **Ni-SU** to **Ni-SI** is a slow process and might involve the loss of the oxygen-containing bridging ligand.[4] The ^{57}Fe ENDOR measurements[15] suggested that the Fe center has the same formal charge in the three EPR-active states **Ni-A**, **Ni-B**, and **Ni-C**, and that the Ni is in the trivalent state. These and other experiments provide essential information for constructing the molecular structures of the active sites of these six redox states.

On the basis of these experimental results, several theoretical attempts[16−19] to predict the structures of these species and the associated catalytic mechanism have been reported. All used density functional theory (DFT)[20] because DFT methods can treat quite large systems and have accuracy close to the most advanced ab initio methods, which are only applicable to much smaller systems. Pavlov et al.[16] probed possible reaction paths for H_2 activation and proposed that the activation of H_2 is likely to occur at the Fe center. The calculations carried out by De Gioia et al.[17] showed that the active site structures proposed by Dole et al.[13] are in reasonable agreement with available experimental data. Niu, Thomson, and Hall[18] have made the most thorough investigations on the possible structures for **Ni-B**, **Ni-SI**, **Ni-C**, and **Ni-R** by correlating the measured CO frequencies with the calculated CO bond lengths. Amara et al.[19] investigated the possible structures of **Ni-A**, **Ni-SI**, **Ni-C**, and **Ni-R** in a study, where the protein backbone was included in modeling through a hybrid density functional/molecular mechanics method. Despite all these efforts, there is not total agreement concerning the nature of all redox states.

The aim of this work is to characterize the active site of the unready states of *D. gigas* enzyme, **Ni-A** and **Ni-SU**, by performing DFT calculations and correlating the calculated CO bond lengths with experimental CO frequencies. Previous geometry optimizations of **Ni-A** assumed that the bridging oxygen-containing ligand is an oxo ligand.[17a,19] However, X-ray crystallography,[1,2] even at a resolution much higher than 2.54 Å, is not able to detect the positions of hydrogen atoms. Therefore, it is unclear whether the bridging ligand of **Ni-A** is oxo or hydroxo. In addition, one (or more) of the cysteine residues of **Ni-A** could be protonated. Furthermore, **Ni-SU** has not been explored by theoretical calculations. The characterization of **Ni-A** and **Ni-SU** should help us understand the activation step of the enzyme and provide verification of the structures of **$Ni\text{-}SI_{1914}$** and **$Ni\text{-}SI_{1934}$**, which are critical for understanding the catalytic cycle of *D. gigas* hydrogenase.

Computational Details

The first step to computationally model the active sites of *D. gigas* enzyme is to choose appropriate active site models for various enzyme forms. Although the protein backbone was found to have some influence on the active site,[19] it is generally believed that the key features of various redox states can be obtained without including the protein in modeling the hydrogenase.[16,17,21] So in our calculations, we neglect the protein backbone and replace the four cysteine groups of the protein with SCH_3 groups. This has proved to be a very effective technique in obtaining active site geometries that can be correlated with the measured CO frequencies.[18]

All the calculations have been performed with the Gaussian 98[22] package. Density functional theory is employed with the three-parameter hybrid exchange functional of Becke[23] and the Lee, Yang, and Parr correlation functional[24] (B3LYP). Relativistic effective core potentials (ECPs)[25] for iron, nickel, and sulfur are employed in all B3LYP calculations. In the ECP for Fe and Ni, the 3s and 3p orbitals are treated explicitly along with the 3d, 4s, and 4p valence orbitals. The basis set for Fe and Ni is a modified LANL2DZ double-ζ basis set plus an f-type polarization function,[26] (341/341/41/1), in which the two 4p functions of the standard LANL2DZ[27] have been replaced by a (41) split of the optimized 4p function from Couty and Hall.[28] For S, the standard LANL2DZ basis set is augmented by a d-type polarization function.[29] For the CO and two CN^- ligands coordinated to the Fe center, and the bridging oxygen atom, a 6-31G(d) basis set[30] is employed. The hydrogen atoms bonded to the bridging oxygen atom and sulfur atoms, and the carbon atoms in SCH_3 groups, have a 3-21G basis set.[31] For these hydrogen atoms in the SCH_3 groups, an STO-3G is used.[32]

(15) Huyett, J. E.; Carepo, M.; Pamplona, A.; Franco, R.; Moura, I.; Moura, J. J. G.; Hoffman, B. M. *J. Am. Chem. Soc.* **1997**, *119*, 9291.
(16) (a) Pavlov, M.; Siegbahn, P. E. M.; Blomberg, M. R. A.; Crabtree, R. H. *J. Am. Chem. Soc*. **1998**, *120*, 548. (b) Pavlov, M.; Blomberg, M. R. A.; Siegbahn, P. E. M. *Int. J. Quantum Chem*. **1999**, *73*, 197.
(17) (a) De Gioia, L.; Fantucci, P.; Guigliarelli, B.; Bertrand, P. *Inorg. Chem*. **1999**, *38*, 2658. (b) De Gioia, L.; Fantucci, P.; Guigliarelli, B.; Bertrand, P. *Int. J. Quantum Chem*. **1999**, *73*, 187.
(18) Niu, S.; Thomson, L. M.; Hall, M. B. *J. Am. Chem. Soc.* **1999**, *121*, 4000.
(19) Amara, P.; Volbeda, A.; Fontecilla-Camps, J. C.; Field, M. J. *J. Am. Chem. Soc*. **1999**, *121*, 4468.
(20) Parr, R. G.; Yang, W. *Density-functional theory of atoms and molecules*; Oxford University Press: Oxford, 1989.
(21) Siegbahn, P. E. M.; Blomberg, M. R. A. *Annu. Rev. Phys. Chem.* **1999**, *50*, 221.
(22) Frisch, M. J.; Trucks, G. W.; Schlegel, H. B.; Scuseria, G. E.; Robb, M. A.; J. R. Cheeseman, J. R.; Zakrzewski, V. G.; Montgomery, J. A., Jr.; Stratmann, R. E.; Burant, J. C.; Dapprich, S.; Millam, J. M.; Daniels, A. D.; Kudin, K. N.; Strain, M. C.; Farkas, O.; Tomasi, J.; Barone, V.; Cossi, M.; Cammi, R.; Mennucci, B.; Pomelli, C.; Adamo, C.; Clifford, S.; Ochterski, J.; Petersson, G. A.; Ayala, P. Y.; Cui, Q.; Morokuma, K.; Malick, D. K.; Rabuck, A. D.; Raghavachari, K.; Foresman, J. B.; Cioslowski, J.; Ortiz, J. V.; Stefanov, B. B.; Liu, G.; Liashenko, A.; Piskorz, P.; Komaromi, I.; Gomperts, R.; Martin, R. L.; Fox, D. J.; Keith, T.; Al-Laham, M. A.; Peng, C. Y.; Nanayakkara, A.; Gonzalez, C.; Challacombe, M.; Gill, P. M. W.; Johnson, B. G.; Chen, W.; Wong, M. W.; Andres, J. L.; Gonzalez, C.; Head-Gordon, M.; Replogle, E. S.; Pople, J. A. *Gaussian 98*; Gaussian, Inc.: Pittsburgh, PA, 1998.
(23) (a) Becke, A. D. *Phys. Rev.* **1988**, *A38*, 3098. (b) Becke, A. D. *J. Chem. Phys.* **1993**, 98, 1372. (c) Becke, A. D. *J. Chem. Phys*. **1993**, *98*, 5648.
(24) Lee, C.; Yang, W.; Parr, R. G. *Phys. Rev.* **1988**, *B37*, 785.
(25) (a) Hay, P. J.; Wadt, W. R. *J. Chem. Phys.* **1985**, *82*, 299. (b) Wadt, W. R.; Hay, P. J. *J. Chem. Phys.* **1985**, *82*, 284.
(26) Ehlers, A. W.; Böhme, M.; Dapprich, S.; Gobbi, A.; Höllwarth, A.; Jonas, V.; Köhler, K. F.; Stegmann, R.; Veldkamp, A.; Frenking, G. *Chem. Phys. Lett.* **1993**, *208*, 111.
(27) LANL2DZ: Dunning D95 basis sets on first row, Los Alamos ECP plus double-ζ basis sets on Na−Bi.
(28) Couty, M.; Hall, M. B. *J. Comput. Chem.* **1996**, *17*, 1359.
(29) Höllwarth, A.; Böhme, M.; Dapprich, S.; Ehlers, A. W.; Gobbi, A.; Jonas, V.; Köhler, K. F.; Stegmann, R.; Veldkamp, A.; Frenking, G. *Chem. Phys. Lett.* **1993**, *208*, 237.
(30) Harihan, P. C.; Pople, J. A. *Theor. Chim. Acta* **1973**, *28*, 213.
(31) Hehre, W. J.; Radom, L.; Schleyer, P. v. R.; Pople, J. A. *Ab initio molecular orbital theory*; Wiley: New York, 1986.
(32) Hehre, W. J.; Stewart, R. F.; Pople, J. A. *J. Chem. Phys.* **1969**, *51*, 2657.

Scheme 2

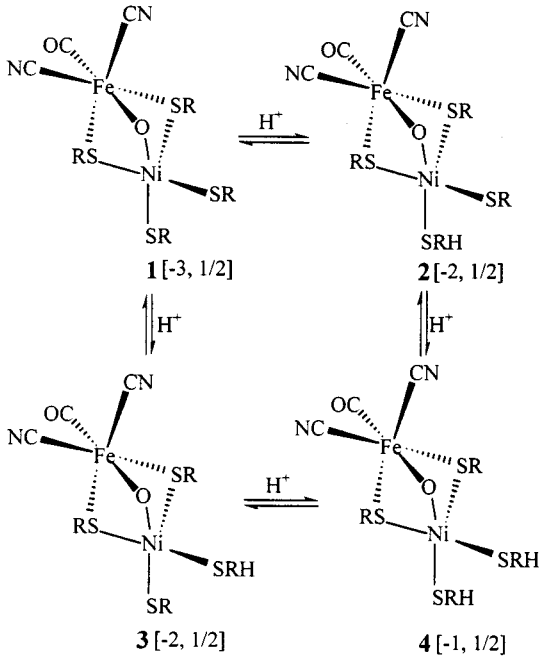

Although a relatively large basis set is chosen for these active site models, the calculated CO stretching frequencies are not yet accurate enough to directly compare with corresponding experimental frequencies. For example, the frequency of free CO at the B3LYP/6-31G(d) level is calculated to be 2208 cm^{-1}, 65 cm^{-1} higher than the experimental value of 2143 cm^{-1}.[33] A straightforward way to improve the accuracy of calculated CO frequencies is to scale the calculated frequencies with the scaling factor obtained for some organometallic model complexes containing an Fe(II)−CO bond, electronically similar to the active site of *D. gigas* hydrogenase. Such model complexes, $CpFe(CN)_2(CO)^-$, $CpFe(CN)(CNCH_3)(CO)$, $CpFe(CNCH_3)_2(CO)^+$, and $Cp^*Fe(CN)_2(CO)^-$, have been synthesized, and their CO frequencies are known.[34,35] For these compounds, we have obtained their B3LYP-optimized structures and performed analytical frequency calculations at these structures (the basis set for hydrogen atoms and carbon atoms in methyl groups of Cp* is 3-21G; for other atoms the same basis set as described above is used). Our calculations show that there exists an excellent linear relationship between the calculated CO frequencies and corresponding experimental values (in CH_3CN), $\nu(CO)^{Exp} = 229.9 + 0.83383\nu(CO)^{Calc}$, with a correlation coefficient (R^2) of 0.989. Besides this scaling method, a simpler method for predicting the CO frequencies in systems with a single Fe−CO bond is based on the recognition that the CO frequency is proportional to the CO bond length.[18,36] An excellent correlation between the optimized CO bond lengths and the natural logarithm of corresponding experimental frequencies, $\ln \nu(CO)^{Exp} = 10.706 - 2.7028 r_{CO}^{Calc}$, with a correlation coefficient (R^2) of 0.980, is found for these model compounds. Therefore, we have two strategies available to give relatively accurate predictions of the CO stretching frequencies in various active site models: (1) scale the directly calculated CO frequencies; (2) use the optimized CO bond lengths for predicting CO frequencies. We will prefer the second method (unless stated explicitly) because it is simpler and gives predictions almost identical with those of the first one.

It should be mentioned that the slope and intercept of the above bond length/frequency relationship are different from those derived in previous work,[18] because the basis set used here is larger than that used previously. This basis set is expected to produce bond lengths in better agreement with the experimental values and therefore give more accurate predictions of CO frequencies in organometallic model complexes and active site models.

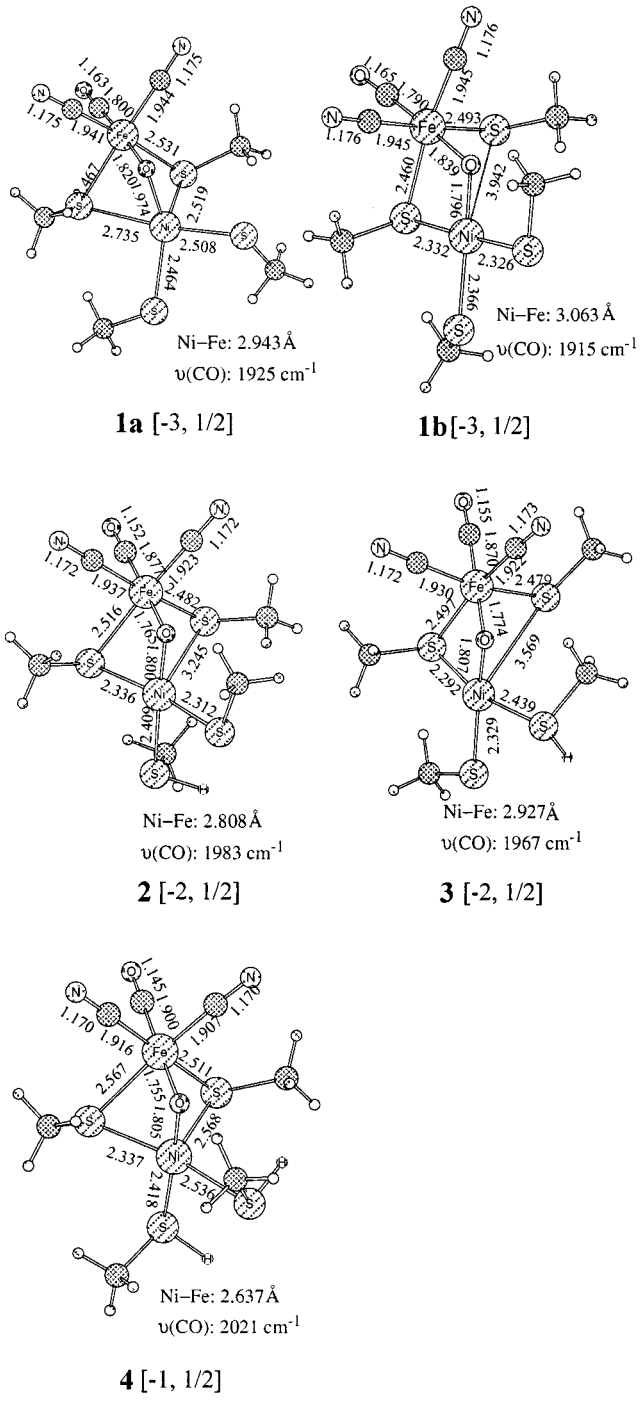

Figure 2. B3LYP-optimized structures of candidates **1a**,**b** and **2**−**4** for **Ni-A**.

Results and Discussion

To assign the correct structures to **Ni-A** and **Ni-SU**, it is important to reconcile some of their properties with available experimental facts:

(1) For **Ni-A**, the unpaired electron should be mainly localized on the Ni center, while **Ni-SU** should be diamagnetic.[5−9]

(2) For **Ni-A**, the optimized structure should be in good agreement with the X-ray structure of *D. gigas* enzyme, in which

(33) Herzberg, G. *Molecular Spectra and Molecular Structure I. Spectra of Diatomic Molecules*; D. Van Nostrand Company, Inc.: New York, 1957.
(34) Darensbourg, D. J.; Reibenspies, J. H.; Lai, C.-H.; Lee, W.-Z.; Darensbourg, M. Y. *J. Am. Chem. Soc.* **1997**, *119*, 7903.
(35) Lai, C.-H.; Lee, W.-Z.; Miller, M. L.; Reibenspies, J. H.; Darensbourg, D. J.; Darensbourg, M. Y. *J. Am. Chem. Soc.* **1998**, *120*, 10103.
(36) (a) Morrison, S. L.; Turner, J. J. J. *J. Mol. Struct.* **1994**, *39*, 317. (b) Zaric, S.; Couty, M.; Hall, M. B. *J. Am. Chem. Soc.* **1997**, *119*, 2885.

Table 1. Mulliken Spin Densities in Various Active Site Models **1a**−**8** for **Ni**−**A**[a]

	1a	1b	2	3	4	5	6	7	8
Ni	1.517	0.147	−0.025	−0.015	−0.032	0.919	0.829	1.445	−0.071
Fe	−0.249	0.244	0.673	0.717	0.813	−0.020	−0.093	−1.073	1.066
S_b(L)	0.044	−0.010	0.018	−0.008	−0.003	−0.055	−0.062	0.195	0.160
S_b(R)	0.078	0.070	0.073	0.097	0.143	0.238	0.334	0.076	−0.051
S_t(R)	0.114	0.006	0.025	−0.003	0.048	−0.077	−0.037	0.055	0.043
S_t(L)	0.069	−0.001	−0.002	−0.002	−0.001	−0.044	0.005	0.180	−0.016
O_b	−0.620	0.604	0.317	0.304	0.249	0.037	0.016	0.058	−0.074
$\langle S^2 \rangle$	1.762	0.771	0.975	1.074	1.294	0.843	0.865	1.781	1.604

[a] S_b and S_t are bridging and terminal sulfur ligands, respectively. L(R) means the sulfur atom on the left (right) side of the structures, **1a**−**8**, given in Figures 2 and 3. O_b is the bridging oxygen atom.

Scheme 3

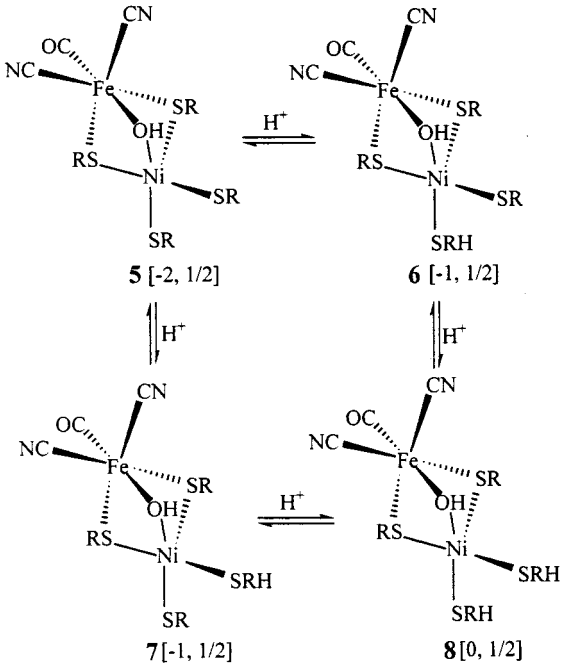

Ni-A is thought to be the single largest component, but which has some **Ni-B** and is ∼50% EPR silent[1,2]

(3) The predicted CO frequencies should be close to the measured values,[4] 1947 cm^{-1} in **Ni-A** and 1950 cm^{-1} in **Ni-SU**. However, considering that the environment of the binuclear Ni−Fe active site in the enzyme is influenced by the protein backbone, the hydrogen bonding to the CN^- ligands, and water molecules, we would not expect that the predicted CO frequencies of active site models would be, in absolute magnitude, exactly the same as corresponding experimental values even if the correct models are assigned. This means that a systematic error should be taken into account. Our limited experience[18,37] would suggest that the predicted frequencies based on organometallic models would be somewhat larger than those measured for the enzyme. However, since our experience is very limited, we will only assume that our predictions should be within ±30 cm^{-1} of the measured CO frequencies in the enzyme. Accordingly, for **Ni-A** and **Ni-SU** those structures with predicted frequencies of $\nu(CO) = 1947 \pm 30$ cm^{-1} and $\nu(CO) = 1950 \pm 30$ cm^{-1}, respectively, will be considered as potential candidates.

(4) In the reduction of **Ni-A** to **Ni-SU** (one proton and one electron are involved, as shown in Scheme 1), the most plausible mechanism, we think, is that the proton goes to the bridging X ligand. The reason is that the conversion from **Ni-SU** to **Ni-SI** likely involves the removal of the bridging X ligand, as suggested by IR experiments,[4] and protonating the X ligand will weaken its bond(s) to the metal(s).

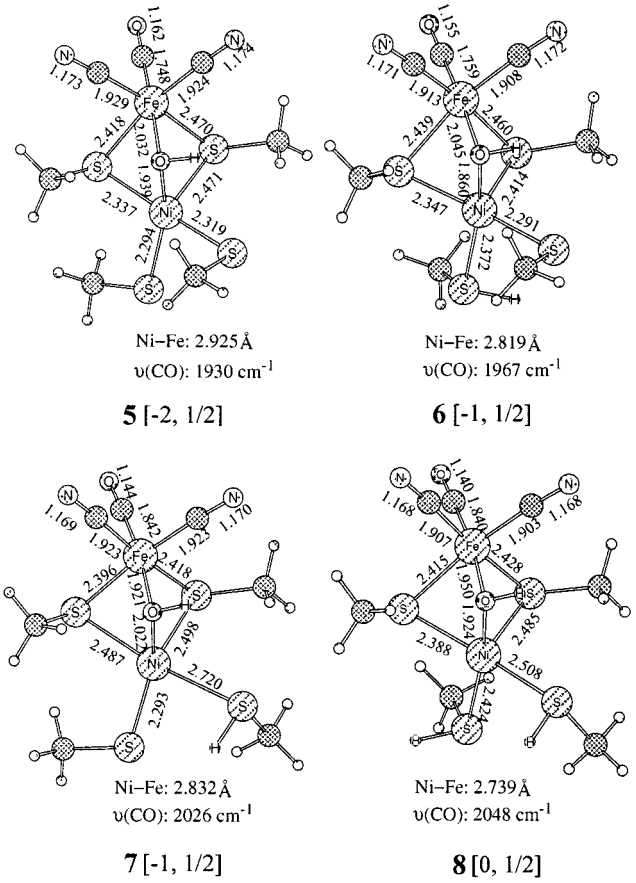

Figure 3. B3LYP-optimized structures of candidates **5**−**8** for **Ni-A**.

In the following, the results and discussion of various models for **Ni-A** are given first**,** followed by those for **Ni-SU**.

Ni-A with Oxo as the X Ligand. EPR[5−9] and ENDOR[15] experiments indicated that **Ni-A** almost certainly corresponds to a Ni(III)−Fe(II) species. Previous calculations showed that protonation on a bridging sulfur atom leads either to unrealistic changes in the coordination sphere of the metal ions[16] or to a structure much less stable than that from protonation on a terminal sulfur.[18] So in our calculations, we only need to consider those candidates with 0, 1, or 2 protons on the terminal sulfur atoms. These **Ni-A** candidates are shown in Scheme 2 and are labeled **N** [*q*, *S*], where **N** is the species, *q* the overall charge, and *S* the total spin. **1** is the unprotonated species, **2** and **3** are protonated on only one of the terminal sulfur atoms, and **4** has both terminal sulfur atoms protonated. The B3LYP-optimized geometries of **1**−**4** are displayed in Figure 2 (the CO frequency, predicted by the bond length/frequency relationship derived in the preceding section, is also given for each species).

(37) Cao, Z.; Hall, M. B. *J. Am. Chem. Soc.*, submitted.

Scheme 4

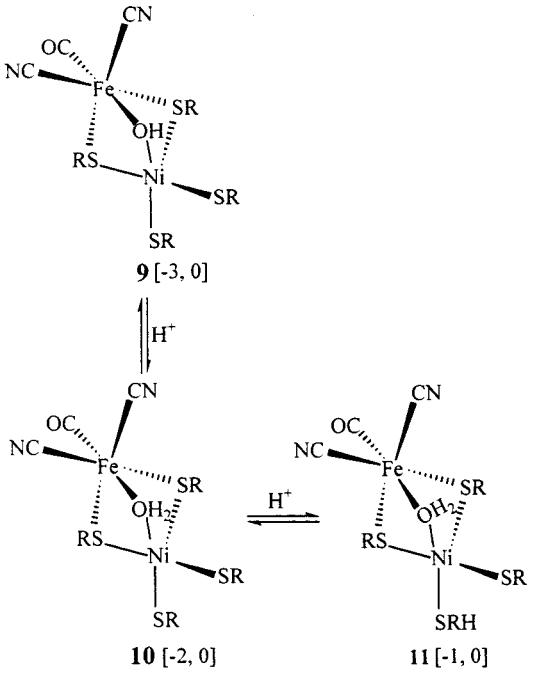

Interestingly, full geometry optimizations starting with two slightly different structures for **1** resulted in two different converged structures, **1a** and **1b**. The spin density distributions for **1a**−**4** are reported in Table 1.

Among the five optimized structures shown in Figure 2, the unprotonated structure, **1a**, is the one that is most similar to the X-ray structure. Like the X-ray structure, **1a** has an octahedral Fe center and a square-pyramidal Ni center with a vacancy trans to one of the bridging sulfur atoms. The calculated Ni−Fe distance, 2.943 Å, is also very close to the experimental value 2.900 Å. Although the spin contamination in **1a** is severe ($\langle S^2 \rangle = 1.762$), the spin-density distribution shows that the unpaired electron is mainly localized on the Ni center (1.517e) and the bridging oxygen atom (−0.620e). In addition, the predicted ν-(CO) in **1a** is 1925 cm^{-1}, within acceptable range of the experimental value. However, the bridging oxygen atom in **1a** is significantly closer to Fe than to Ni, a result inconsistent with the experimental observation. Furthermore, **1b** is 2.4 kcal/mol more stable than **1a**.

In **1b**, the bridging oxygen ligand is closer to the Ni atom, but the unpaired electron is mainly on O_{bridge} (0.604e) and one of Ni−S_{bridge} bonds is totally broken. The predicted CO frequency for **1b**, 1915 cm^{-1}, is also beyond the acceptable range. On the basis of the predicted CO frequencies (1983 $cm^{-1}$for **2**, 1967 cm^{-1} for **3**), **3** is acceptable for **Ni-A** but **2** is not. However, both **2** and **3** have large Fe spin densities and long Ni−S_{bridge} bond length, characteristics that eliminate both as suitable models for **Ni-A**. Although **4** is geometrically similar to **1a**, the large spin density on Fe and the high predicted CO frequency preclude **4** as an appropriate model for **Ni-A**.

Ni-A with Hydroxo as the X Ligand. Candidates for **Ni-A** with a μ-hydroxo ligand are shown in Scheme 3. Like the systems discussed above, these species are unprotonated (**5**), singly protonated (**6** and **7**), and doubly protonated (**8**) on the terminal sulfur(s). The B3LYP-optimized geometries of **5**−**8** are shown in Figure 3. The spin density distributions in **5**−**8** are also collected in Table 1.

In the unprotonated structure **5**, the Ni−Fe distance is 2.925 Å, the bridging hydroxo ligand is closer to Ni (1.939 Å) than

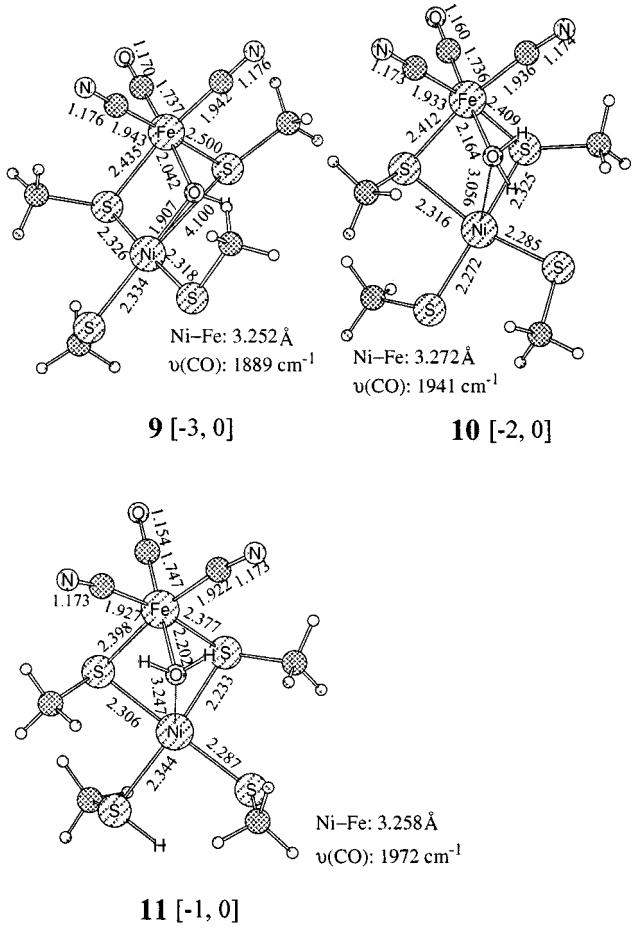

Figure 4. B3LYP-optimized structures of candidates **9**−**11** for **Ni-SU**.

to Fe (2.032 Å), and the remaining geometrical features are in good agreement with the X-ray structure obtained for *D. gigas* hydrogenase. The spin density on **5** is localized mainly on the Ni atom (0.919e) and one of the bridging S atoms (0.238e), a result compatible with EPR experiments of **Ni-A**. Both methods for predicting the CO frequency yield results that are similar (1930 and 1925 cm^{-1}) and in agreement with the experimental frequency of **Ni-A**. These results are strong support for **5** as the appropriate model for **Ni-A**.

However, the singly protonated species **6** appears to be a competitive model for **Ni-A** and shows structural features similar to those of **5** except that the Ni−Fe distance (2.819 Å) is 0.106 Å shorter and the CO bond length (1.155 Å) is 0.007 Å shorter. The predicted CO frequency, 1967 cm^{-1}, is within the acceptable range. The spin density distribution on **6** is also very similar to that on **5**.

Another singly protonated species, **7**, seems an unlikely candidate for **Ni-A**. First, the Ni−S bond between the Ni and the protonated terminal sulfur is 0.52 Å longer than the experimentally measured value. Second, the calculated CO bond length is only 0.005 Å longer than that of free CO, leading to a very high predicted CO frequency, 2026 cm^{-1}, far beyond the acceptable range.

Species **8** has both terminal sulfur atoms protonated. The calculated Ni−Fe bond distance (2.739 Å) is 0.16 Å shorter than the experimental value. The CO bond length is calculated to be 1.140 Å, like **7**, close to that of free CO, and the CO frequency is predicted to be the highest among these hydroxo

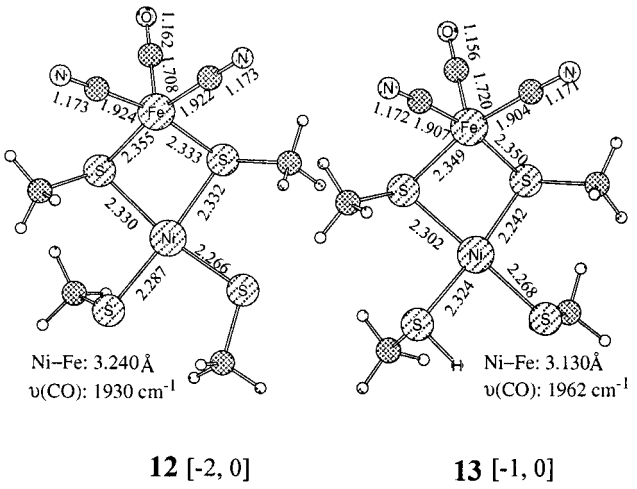

Figure 5. B3LYP-optimized structures of **12** (candidate for **Ni-SI$_{1914}$**) and **13** (candidate for **Ni-SI$_{1934}$**).

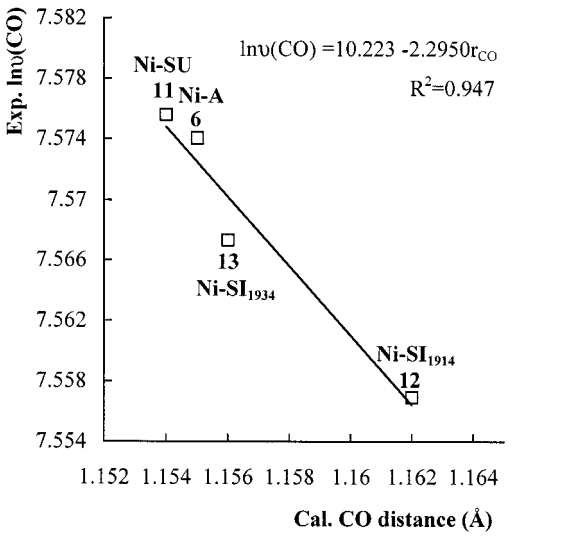

Figure 6. Relationship between the optimized CO bond lengths and experimental frequencies[4] of the intermediates of *D. gigas* hydrogenase.

models (**5**−**8**). Clearly, these characteristics eliminate **8** as a suitable model for **Ni-A**.

Generally, the CO distance and the Ni−Fe distance become gradually shorter as the degree of protonation of the terminal sulfur atoms is increased. This trend was observed previously[18] in an investigation of the structures of active site models for **Ni-B**, **Ni-SI**, **Ni-C**, and **Ni-R**. From the above discussions, we conclude that three structures, **1a** (with the μ-oxo bridge) and **5** and **6** (both with the μ-hydroxo bridge), could be considered as suitable models for **Ni-A**. However, the following discussions on **Ni-SU** will further narrow the possible models for **Ni-A** since the correct model for **Ni-A** must correlate with the interpretation of the observed transition from **Ni-A** to **Ni-SU**.[4]

Ni-SU. Three potential candidates for **Ni-SU**, **9**−**11**, are constructed by reducing Ni(III) to Ni(II) and protonating the μ-oxo ligand of **1a** and the μ-hydroxo ligand of **5** and **6**, respectively (Scheme 4). Their B3LYP-optimized structures are displayed in Figure 4.

In **9**, one of Ni−S$_{bridge}$ bonds is completely broken and the predicted decrease of ν(CO) from **1a** to **9** (36 cm^{-1}) cannot be reconciled with the 3 cm^{-1} increase observed from **Ni-A** to **Ni-SU**. Additionally, the bridging hydroxo ligand will be very difficult to remove since it is covalently bonded to Fe and Ni. Thus, **9** can be excluded as a suitable model of **Ni-SU**, implying that **1a** would not be a good model for **Ni-A**.

Both species **10** and **11** show a square-planar Ni and an octahedral Fe. The water molecule generated from protonating the μ-hydroxo ligand is only bonded to the Fe center in these two species. The Ni−Fe distance in **10** and **11** is lengthened by 0.347 and 0.427 Å, relative to **5** and **6**, respectively. Although the protein may prevent the full expansion of the Ni−Fe bond length, previous work[18] has shown that the CO frequency, one of our key links to the experiments, depends only weakly on this distance. Experimentally, the CO frequency is increased by 3 cm^{-1} in going from **Ni-A** to **Ni-SU**, while the predicted ν(CO) increase is 11 cm^{-1} for **5** to **10**, and 5 cm^{-1} for **6** to **11**. Therefore, on the basis of the known experimental information about the **Ni-A**/**Ni-SU** transition, it is still difficult to judge which one (**10** or **11**) is a better model for **Ni-SU**.

In order to resolve this ambiguity, we can examine the **Ni-SU**/**Ni-SI** transformation. IR experiments[4] suggested that the **Ni-SU**/**Ni-SI** transformation is slow and might involve the loss of the bridging ligand, as **Ni-SI** reacts rapidly with H_2. In our calculations, the conversion from **Ni-SU** to **Ni-SI** requires the coordinated water molecule to be eliminated. **Ni-SI** exists in two forms,[4] and according to our previous work[18] **Ni-SI$_{1914}$** is unprotonated and **Ni-SI$_{1934}$** is singly protonated on the terminal sulfur. If **10** is **Ni-SU**, eliminating the water molecule from **10** leads to species **12** for **Ni-SI$_{1914}$** since none of the cysteine ligands are protonated in **10**. But if **11** is **Ni-SU**, eliminating the water molecule from **11** leads to **13** for **Ni-SI$_{1934}$**.

The optimized structures for **12** and **13** are shown in Figure 5, structures which are similar to those previously predicted[18] to be the correct models for **Ni-SI$_{1914}$** and **Ni-SI$_{1934}$**, respectively. Species **12** and **13** are structurally very similar to **10** and **11**, respectively. The binding energy between the water molecule and the Fe center is calculated to be 22.5 kcal/mol in **10**, and 21.2 kcal/mol in **11** (the basis set superposition error is not included). These results are in reasonable accord with the fact that the rate-determining step for activation of *D. gigas* hydrogenase is a slow process in which **Ni-SU** is converted into **Ni-SI**.[4] However, the ν(CO) shift from **10** to **12** is predicted to be −11 cm^{-1}, while the experimental ν(CO) shift from **Ni-SU** to **Ni-SI$_{1914}$** is −36 cm^{-1}. The poor agreement between the calculated and observed ν(CO) changes indicates that the assignment of **10** to **Ni-SU** and, correspondingly, **5** to **Ni-A** is questionable. On the other hand, the ν(CO) shift from **11** to **13** is predicted to be −10 cm^{-1}, a value in good agreement with the experimental shift of −16 cm^{-1} from **Ni-SU** to **Ni-SI$_{1934}$**.

Thus, our final models for **Ni-A** and **Ni-SU** are **6** and **11**, respectively. These predictions are internally consistent with **12** being **Ni-SI$_{1914}$** and **13** being **Ni-SI$_{1934}$**, as predicted previously.[18]

Conclusions

Density functional calculations have successfully predicted the structures and CO stretching frequencies of the observed states of [NiFe] *D. gigas* hydrogenase. **Ni-A** has been identified as a Ni(III)−Fe(II) species with a hydroxo bridge and a protonated terminal cysteine (**6**). The fully optimized structure shows remarkable agreement with the X-ray structure, including a square-pyramidal Ni with a vacant coordination site trans to a bridging S. The **Ni-A** to **Ni-SU** transformation corresponds to reduction of Ni and protonation of the bridging hydroxo, which produces a Ni(II)−Fe(II) species with a H_2O coordinated to Fe. When this H_2O molecule dissociates, the system transforms to **Ni-SI$_{1934}$**.

Finally, for the active site models identified here**, Ni-A**, **Ni-SU**, **Ni-SI$_{1914}$**, and **Ni-SI$_{1934}$**, a very good correlation between their calculated CO distances and the natural logarithm of corresponding measured CO frequencies, as shown in Figure 6, corroborates our assigned structures. This relationship is very similar to that derived from the organometallic model complexes. The slight difference reflects the fact that the environment of the $Fe(CN)_2(CO)$ unit in the enzyme is somewhat different from that in the selected organometallic model complexes, as explained in a preceding section.

Acknowledgment. We would like to thank National Science Foundation (Grant CHE 9800184) and the Robert A. Welch Foundation (Grant A-648) for their generous support.

IC0001715